Modeling for Local Dynamic Behaviors of Phenol Biodegradation in Bubble Columns

Wei Feng, Jianping Wen, Xiaoqiang Jia, Qing Yuan, Yan Sun
Dept. of Biochemical Engineering, School of Chemical Engineering and Technology, Tianjin University, 92 Weijin Road, Nankai District, Tianjin 300072, China

Cuiyun Liu
Key Lab of Polymer Science and Nanotechnology, Henan University of Science and Technology, Luoyang, 471003, China

DOI 10.1002/aic.10899
Published online June 9, 2006 in Wiley InterScience (www.interscience.wiley.com).

A coupled three-dimensional (3-D) model, combining hydrodynamics with biochemical reactions, was developed to simulate the local transient flow patterns and the dynamic behaviors of cell growth and phenol biodegradation by yeast Candida tropicalis *in the bubble-column bioreactor, using the computational fluid dynamic (CFD) method. In order to validate this proposed model effectively, the validation of the local hydrodynamic characteristics of the gas-mineral salt solution (gas-liquid) two-phase system, with the phenol concentration of 1200 mg/L, and with the absence of cells, was performed in a square-sectioned bubble column bioreactor using the LDA system and conductivity probe. Furthermore, the validation of phenol biodegradation behaviors by yeast* Candida tropicalis *at different initial concentrations of phenol and cell was also carried out in the above bubble-column bioreactor. The results indicated that the model simulations had a satisfying agreement with the experimental data. Finally, the local instantaneous flow and phenol biodegradation features including gas holdup, gas velocity, liquid velocity, cell concentration and phenol concentration inside the bioreactor were successfully predicted in different-scale bubble columns by the proposed model.* © 2006 American Institute of Chemical Engineers *AIChE J,* 52: 2864–2875, 2006
Keywords: hydrodynamics, CFD, modeling, phenol, bubble column, candida tropicalis

Introduction

As a high-toxic organic compound even at low-concentration and one of the most common water pollutants, phenol is contained in the effluents of several industries and operations, such as petroleum refineries, gas and coke oven industries, fiberglass units, pharmaceuticals, explosive manufacture, phenolic resin manufacture, plastic and varnish industries, textiles units and metallurgical operations. If these hazard effluents are directly discharged into drinking water sources, they would negatively affect water quality and public health. Therefore, it has been mandatory to treat these wastes before safe disposal to the water, and the World Health Organization (WHO) has set a limit of 1 mg/L to regulate the phenol concentration in the drink water.[1-3]

The most common method developed to deal with the removal of phenol from wastewater is biological treatment,[4-8] which is generally preferred to physical or chemical treatment methods due to lower costs and possibility of complete mineralization.[9] Although the biological treatment of phenolic wastewater can be achieved with conventional activated sludge systems, such systems have been known to be easy to break down because of fluctuations in phenol loads or exposure to high-phenol loading.[10] Thus, various pure cultures of microbial

Correspondence concerning this article should be addressed to J. Wen at jpwen@tju.edu.cn.

strains have been tested for degrading phenolic compounds.[11-14] Among these pure cultures, Jiang et al.[15] isolated a strain of yeast *Candida tropicalis,* and showed that it could degrade very high-concentration phenol up to 2,000 mg/L.

Because of their simple construction, bubble-column bioreactors have received increasing interests and wide utilization in both fermentation processes and wastewater treatments. They provide several advantages during operation and maintenance, such as high-heat and mass-transfer rates, compactness and low-operating and maintenance costs. Recently, the investigations of phenolic wastewater treatment employing bubble-column bioreactors have been performed.[16-19] Ruiz-Ordaz et al.[18] documented that high-strength phenol was biodegraded using a repeated batch culture of *Candida tropicalis* in a multistage bubble column bioreactor. The phenol removal efficiencies obtained with this system were higher than 98.7%. Tay et al.[19] reported the high-rate biodegradation of toxic phenol by aerobically grown microbial granules in a bubble-column bioreactor with a sequencing batch model. They found that phenol was completely degraded and high-biomass concentration was maintained in the reactor even at a high-phenol loading of 2.5 kg/d·m^3. Gonzalez et al.[16] reported their experimental investigation of continuous biodegradation processes treating phenol using *Pseudomonas putida* in the stirred-tank bioreactor with free cells, and in the bubble-column bioreactor with immobilized cells. Experimental values indicated that the bubble-column bioreactor system showed better performance than that of the stirred-tank bioreactor system due to its better control and lower hydraulic residence time (HRT).

Knowledge of kinetics of phenol biodegradation is necessary for improvements in the process control and phenol removal efficiency. To evaluate the relationship between the specific degradation rate and the phenol concentration, kinetics of phenol biodegradation and cell growth have been investigated extensively. Monteiro et al.[20] studied the kinetics of phenol biodegradation in a batch reactor using a pure culture of *Pseudomonas putida* DSM 548. Nuhoglu and Yalcin[2] determined a new kinetic model including Haldane and an alternative one to simulate the phenol removal profiles with time. Jiang et al.[15] investigated the cell growth and phenol degradation intrinsic kinetics of yeast *Candida tropicalis* in batch cultures over a wide range of initial phenol concentrations (0–2,000 mg/L). However, investigations of the kinetics coupling with hydrodynamics in bubble-column bioreactors are very limited. Livingston and Chase[21] proposed a mathematical model, regarding the reactor as a fully-mixed one, for describing simultaneous diffusion and reaction of oxygen and phenol in the bubble column with a draft tube. They used this model to discuss the transition from phenol-limited to oxygen-limited kinetics of phenol biodegradation. However, this model did not consider the effects of the local hydrodynamics on the dynamic behaviors of phenol biodegradation.

Due to the complex hydrodynamics and corresponding influence on reaction characteristics, the local dynamic behaviors of phenol biodegradations in the bubble column bioreactors are still not well understood. As a result, a detail CFD model investigation and an improved understanding of the flow, bioreaction and their interactions in the processes of phenol biodegradations are very necessary.

The aim of this work is first to establish a coupled 3-D model for simulating the hydrodynamic characteristics and batch-phenol biodegradation behaviors in the bubble-column bioreactor using CFD method; and then to experimentally perform hydrodynamics and batch phenol biodegradation investigations, respectively, to validate the developed model; and finally to predict the transient hydrodynamics and phenol biodegradation behaviors of different-scale bubble columns using this proposed model.

Model development

In this work, a 3-D model describing the hydrodynamics and the biodegradation behaviors of phenol by *Candida tropicalis* in the bubble-column bioreactor was established. The Euler approach was used to describe the flow and bioreaction characteristics in the bubble column bioreactor. In order to effectively establish the 3-D model for local phenol biodegradation behaviors, some assumptions were made as follows:

1. The initial phenol and cell concentrations in the liquid phase were uniform, and flows in the bubble column bioreactor were assumed to be a two-phase system containing the liquid mixture phase and gas phase.
2. Substrate biodegradation and cell growth were only limited by phenol in the free cells system, while all other nutrients including oxygen were in excess.
3. Fluid flow and bioreaction were coupled and interacted with each other. Fluid flow affected the bioreaction, leading to the change of the liquid physical properties of the fermentation broth, which will in turn affect the hydrodynamic characteristics.

Based on a 3-D two-phase fluid dynamic model,[22,23] and considering the earlier assumptions, time-series momentum equations and continuity equations were applied for developing a 3-D fluid dynamic model with shear-stress transport (SST) turbulence model included, and time-series species transport equation was used for developing the mass balance model.

Continuity and momentum equations

In this model, the velocities of the gas and liquid phases were taken into consideration, respectively. The continuity and momentum balance equations for the *i*th phase (gas phase or liquid phase) were given as follow

$$\frac{\partial(\varepsilon_i\rho_i)}{\partial t} + \nabla\cdot(\varepsilon_i\rho_i\mathbf{u}_i) = 0 \tag{1}$$

$$\frac{\partial(\varepsilon_i\rho_i\mathbf{u}_i)}{\partial t} + \nabla\cdot(\varepsilon_i(\rho_i\mathbf{u}_i\mathbf{u}_i)) = -\varepsilon_i\nabla p + \nabla\cdot(\varepsilon_i\mu_{eff,i}(\nabla\mathbf{u}_i + (\nabla\mathbf{u}_i)^T)) + \varepsilon_i\rho_i\mathbf{g} \pm \mathbf{M}_I \tag{2}$$

where ε_i, the volume fraction of *i*th phase, was related by the following summation constraint

$$\sum_{i=1}^{n}\varepsilon_i = 1 \tag{3}$$

The gas phase was considered as ideal gas, and the density of the gas phase ρ_g was calculated by

$$\rho_g = \frac{\rho_{g,0}[P_0 + \rho_l g(H - Z)(1 - \varepsilon_g)]}{P_0} \cdot \frac{T_0}{T} \tag{4}$$

Interface models

The interface forces between the gas phase and liquid phase have been considered by adding the term $\mathbf{M}_I$ and were calculated by combining proper formulations of interface-force coefficients with the phase velocities. Thus, the two phases (gas and liquid phases) were coupled through the interface forces, and the summation constraint of phase volume fractions (Eq. 3).[24] The similar works also can be found in the literatures of Deen[23] and Delnoij et al.[24]

Jakobsen et al.[25] have discussed these forces extensively, and the term $\mathbf{M}_I$ was composed of drag force, lift force, virtual mass force and turbulent dispersion force, respectively

$$\mathbf{M}_I = \mathbf{M}_D + \mathbf{M}_L + \mathbf{M}_{VM} + \mathbf{M}_{TD} \tag{5}$$

The drag force $\mathbf{M}_D$ was given as

$$\mathbf{M}_D = \frac{3}{4}\frac{C_D}{d_B}\varepsilon_g \rho_l |\mathbf{u}_l - \mathbf{u}_g|(\mathbf{u}_l - \mathbf{u}_g) \tag{6}$$

A variety of models have been proposed for calculating Sauter mean bubble sizes in gas-liquid flow,[26] and the best known and most frequently used model of Calderbank[27] was adopted in this work

$$d_B = 4.15\left(\frac{\sigma_l}{\rho_l}\right)^{0.6} \frac{1}{\varepsilon_g^{0.4}} \tag{7}$$

The drag coefficient C_D for gas-liquid multiphase flow system was taken from Tsuchiya et al.,[28]

$$C_D = \max\left\{\frac{24}{\mathrm{Re}_B}(1 + 0.15\,\mathrm{Re}_B^{0.687}), \frac{8}{3}\left(\frac{E\ddot{o}}{E\ddot{o} + 4}\right)\right\} \tag{8}$$

where

$$\mathrm{Re}_B = |\mathbf{u}_g - \mathbf{u}_l| d_B \rho_l / \mu_l, \text{ and } E\ddot{o} = g\Delta\rho d_B^2/\sigma.$$

The effect of shearing motion in the liquid phase on the movement of the gas phase was modeled by the lift force $\mathbf{M}_L$

$$\mathbf{M}_L = C_L \varepsilon_g \rho_l (\mathbf{u}_l - \mathbf{u}_g) \times (\nabla \times \mathbf{u}_l) \tag{9}$$

The virtual mass force, the acceleration of the liquid phase in the wake of the bubble was taken into account

$$\mathbf{M}_{VM} = -C_{VM}\varepsilon_g \rho_l \left(\frac{D_g \mathbf{u}_g}{Dt} - \frac{D_l \mathbf{u}_l}{Dt}\right) \tag{10}$$

The turbulent dispersion force $\mathbf{M}_{TD}$, which resulted in additional dispersion of phases from high-volume fraction regions to low-volume fraction regions due to turbulent fluctuations, was calculated from Lopez de Bertodano Model[29]

$$\mathbf{M}_{TD} = C_{TD}\rho_l k \nabla \varepsilon_g \tag{11}$$

Turbulence closure

The turbulence was modeled using *SST* model,[30] which worked by solving a turbulence/frequency-based model (k-ω) at the wall and k-ε model in the bulk flow. The robustness optimization have brought the *SST* model to the same level of convergence as the standard k-ε model with wall function, and the improved near-wall formulation has reduced the near wall grid resolution requirement. This model has made its way into most industrial, commercial and many research codes. The equations describing this model were

$$\frac{\partial(\rho_l \kappa)}{\partial t} + \nabla \cdot (\rho_l \mathbf{u}_l \kappa) = \nabla \cdot \left[\left(\mu + \frac{\mu_{T,l}}{\sigma_\kappa}\right)\nabla\kappa\right] + G_{\kappa,l} - \beta' \rho_l \kappa \omega \tag{12}$$

$$\frac{\partial(\rho_l \omega)}{\partial t} + \nabla \cdot (\rho_l \mathbf{u}_l \omega) = \nabla \cdot \left[\left(\mu_{L,l} + \frac{\mu_{T,l}}{\sigma_{\omega 3}}\right)\nabla\omega\right] + (1 - F_1)2\rho_l \frac{1}{\sigma_{\omega 2}} \nabla\kappa\nabla\omega + \alpha_3 \frac{\omega}{\kappa} G_{\kappa,l} - \beta_3 \rho_l \omega^2 \tag{13}$$

where the production of turbulence kinetic energy $G_{k,l}$, was computed from

$$G_{\kappa,l} = \min[\mu_{T,l}(\nabla\mathbf{u}_l + (\nabla\mathbf{u}_l)^T) : \nabla\mathbf{u}_l, 10 \cdot \beta' \rho_l k\omega] \tag{14}$$

and the blending function F_1 was defined by

$$F_1 = \tanh\left\{\left\{\min\left[\max\left(\frac{\sqrt{k}}{\beta'\omega y}, \frac{500\mu_{L,l}}{\rho_l y^2 \omega}\right), \frac{4\rho k}{CD_{kw}\sigma_{\omega 2} y^2}\right]\right\}^4\right\} \tag{15}$$

with $CD_{kw} = \max(2\rho_l(1/\sigma_{\omega 2}\omega)\nabla k \nabla\omega, 1.0 \times 10^{-10})$ and y was the distance to the nearest wall.

The turbulent viscosity was computed from a simple turbulent eddy viscosity model[30]

$$\mu_{T,l} = \frac{\rho_l \alpha_1 k}{\max(\alpha_1 \omega, SF_2)} \tag{16}$$

where S was an invariant measure of the strain rate, and F_2 was a second blending function defined by

$$F_2 = \tanh\left\{\left[\max\left(\frac{2\sqrt{k}}{\beta'\omega y}, \frac{500\mu_{L,l}}{\rho_l y^2 \omega}\right)\right]^2\right\} \tag{17}$$

All constants were computed by a blend from the corresponding constants of the k-ε and k-ω model via $\Phi_3 = F_1\Phi_1 + (1 - F_1)\Phi_2$, and so on. The constants for the earlier equations were: $\beta' = 0.09$, $\alpha_1 = 5/9$, $\beta_1 = 3/40$, $\sigma_{k1} = 0.85$, $\sigma_{\omega 1} = 2$, $\alpha_2 = 0.44$, $\beta_2 = 0.0828$, $\sigma_{k2} = 1$, $\sigma_{\omega 2} = 1/0.856$.[30]

The effective viscosity of the liquid phase in momentum equations was composed of laminar, turbulent and bubble induced viscosity

$$\mu_{eff,l} = \mu_{L,l} + \mu_{T,l} + \mu_{BIT,l} \tag{18}$$

The effective gas viscosity $\mu_{eff,g}$ was based on the effective viscosity of the liquid phase, as was proposed by Jakobsen et al.[25]

$$\mu_{eff,g} = \frac{\rho_g}{\rho_l}\mu_{eff,l} \tag{19}$$

The turbulence induced by the movement of the bubbles was accounted for with the model proposed by Sato et al.[31]

$$\mu_{BIT,l} = C_{\mu,BIT}\varepsilon_g\rho_l d_B|\mathbf{u}_g - \mathbf{u}_l| \tag{20}$$

Species transport equation

The *k***th** species fraction of the phenol biodegradation in the liquid mixture can be represented by the species transport equation of species k

$$\frac{\partial(\varepsilon_l\rho f_k)}{\partial t} + \nabla\cdot(\varepsilon_l\rho_l f_k\mathbf{u}_l) = \nabla\cdot\left(\varepsilon_l\frac{\mu_{eff,l}}{Sc_k}\nabla f_k\right) + \varepsilon_l\gamma_k \tag{21}$$

where f_k was the mass fraction of the *k***th** species in the liquid mixture, and γ_k was the source term accounting for the growth rate or biodegradation rate of *k***th** species.

For a mixture consisting of N species, N-1 transport equations needed to be solved and the overall species balance was given by

$$\sum_{k=1}^{N} f_k = 1 \tag{22}$$

The liquid phase density ρ_l, viscosity μ_l and surface tension σ_l in the bubble-column bioreactor were related to the residual phenol and cell concentrations. Under the condition of the initial phenol concentration varied from 100 to 2,000 mg/L and the initial cell concentration varied from 10 to 102 mg/L, the variables of the liquid physical properties in the phenol biodegradation processes in shaking flasks were experimentally investigated by Cao and Wen[32], and the following expressions have been obtained

$$\frac{\rho_l}{\rho_{l,0}} = 1 + 1\times10^{-6}\frac{S}{[S]} - 4\times10^{-6}\frac{X}{[X]} \qquad (R^2 = 0.972) \tag{23}$$

$$\frac{\mu_l}{\mu_{l,0}} = 1 - 4\times10^{-5}\frac{S}{[S]} - 9\times10^{-9}\left(\frac{S}{[S]}\right)^2 + 1\times10^{-3}\frac{X}{[X]} - 8\times10^{-7}\left(\frac{X}{[X]}\right)^2 \qquad (R^2 = 0.963) \tag{24}$$

$$\frac{\sigma_l}{\sigma_{l,0}} = 1 - 1\times10^{-5}\frac{S}{[S]} - 1\times10^{-8}\left(\frac{S}{[S]}\right)^2 + 5\times10^{-12}\left(\frac{S}{[S]}\right)^3 - 1.2\times10^{-3}\frac{X}{[X]} + 5\times10^{-5}\left(\frac{X}{[X]}\right)^2 - 8\times10^{-8}\left(\frac{X}{[X]}\right)^3 \qquad (R^2 = 0.971) \tag{25}$$

where $\rho_{l,0}$, $\mu_{l,0}$ and $\sigma_{l,0}$ were the liquid density, liquid viscosity and liquid surface tension of the mineral salt medium without phenol and cells. [S] and [X] were the unit concentrations of phenol and cells, respectively.

Intrinsic reaction

Phenol biodegradation by the yeast *Candida tropicalis* has been studied in shaking flasks by Jiang et al.,[15] and the intrinsic cell growth and phenol biodegradation kinetics of the yeast *Candida tropicalis* were determined experimentally

$$\gamma_X = \mu_X\cdot X = \frac{dX}{dt} = \frac{\mu_{\max}S}{K_s + S + \frac{S^2}{K_i}}\cdot X = \frac{0.48S}{11.7 + S + \frac{S^2}{207.9}}\cdot X \qquad (R^2 = 0.996) \tag{26}$$

$$\gamma_S = \mu_S\cdot X = -\frac{dS}{dt} = \alpha\cdot\gamma_X + \beta\cdot X = 0.823\gamma_X + 0.277X \qquad (R^2 = 0.994) \tag{27}$$

Initial and boundary conditions

The initial conditions were specified as follow for $t = 0$

$$\left.\begin{array}{l} u_{g,x} = u_{g,y} = u_{g,z} = 0; \\ u_{l,x} = u_{l,y} = u_{l,z} = 0; \\ \varepsilon_g = 0, \quad \varepsilon_l = 1; \\ f_{phenol} = f_{phenol,0}; \\ f_{cell} = f_{cell,0} \end{array}\right\} \tag{28}$$

At inlet of the column, inlet velocities, volume fractions and species mass fractions in the liquid phase were given

$$\left.\begin{array}{l} u_{g,z} = u_{g,s}\times D\times D/S_{inlet}; \\ u_{g,x} = u_{g,y} = 0; \\ u_{l,x} = u_{l,y} = u_{l,z} = 0; \\ \varepsilon_g = 1, \quad \varepsilon_l = 0; \\ f_{phenol} = f_{cell} = 0 \end{array}\right\} \tag{29}$$

where $u_{g,s}$ and $D\times D$ were the superficial gas velocity and the cross section area of the column, respectively. Along the walls, no-slip boundaries were applied for the liquid phase, while free-slip boundaries were used for the gas phase. Degassing boundary conditions were used at the free surface of outlet.[33]

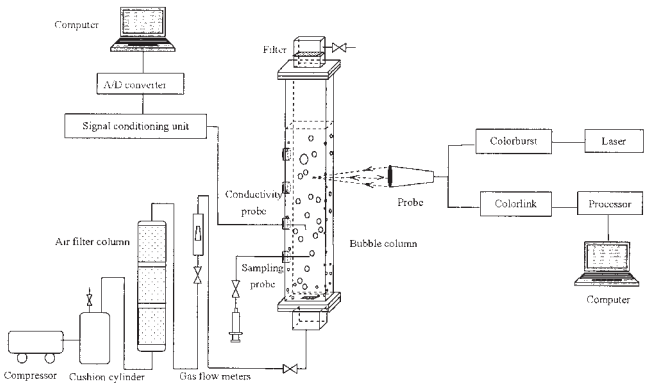

Figure 1. Apparatus.

Numerical implement

In order to numerically solve the system of partial and ordinary differential equations presented above, a "high-resolution" discretisation of the equations has been carried out using a finite volume scheme with a coupled multigrid solver as implemented in the CFD code CFX (http://www.ansys.com/products/cfx.asp). A full-implicit scheme technology was used by solving the full hydrodynamic system of equations simultaneously across all grid nodes. An unstructured numerical grid has been implemented with an average grid cell of $10 \times 10 \times 20$ mm corresponding to a total number of 12000 cells. To save the computing cost, a time-stepping strategy was used in the transient simulations based on the suggestions of Krishna et al.[34] and Feng et al.[35]:100 steps at 0.001 s, 100 steps at 0.002 s, 100 steps at 0.005 s, 100 steps at 0.01 s, 200 steps at 0.02 s, 200 steps at 0.05 s, and for the rest time a time step length of 0.1 s was used. Convergence was good, and a maximum residual convergent goal of 1×10^{-4} was specified in all computations presented here.

Experiment

Experimental setup

The experimental set-up of a Plexiglas rectangle bubble column bioreactor was shown in Figure 1. The Plexiglas rectangle bubble column bioreactor had a cross-section of 0.2×0.2 m, and a height of 1.0 m. The square glass diffuser, centrally located at the bottom of the column, was 50 mm in width and contained 169 holes with a diameter of 1.0 mm. Air filtered by an air filter column was measured by a rotor flowmeter, and then was introduced into the column via the gas diffuser. At the outlet of the column, a filter was used to protect the bubble-column bioreactor from being polluted. The superficial gas velocities varied from 0.01 to 0.02 m/s, which ensure that oxygen was in excess for phenol biodegradation processes, and all local time-averaged gas holdups inside the reactor were lower than 20%.

Hydrodynamic experiments

In order to eliminate the disturbance of fermentation broth on the measurement and to enhance the measurement veracity, measurements of the hydrodynamics were performed in an air-mineral salt medium system including the phenol concentration of 1,200 mg/L and with the absence of cells. The bioreactor was operated under a batch condition with the static liquid height of 0.6 m, and the mineral salt medium contains (g/L): 0.4 K_2HPO_4, 0.2 KH_2PO_4, 0.1 NaCl, 0.1 $MgSO_4$, 0.01 $MnSO_4 \cdot H_2O$, 0.01 $Fe_2(SO_4)_3 \cdot H_2O$, 0.01 $Na_2MoO_4 \cdot 2H_2O$, 0.4 $(NH_4)_2SO_4$. Hydrodynamic experiments were performed under the condition of atmospheric pressure and room temperature. The initial sampling time of experimental measurements was specified at 5 min after the introduction of air into the column when an operating parameter was changed.

Local liquid velocity measurements

Quantitative liquid velocity measurements were performed with a Dantec 3D Laser Doppler Anemometer (LDA) operated in the backward scattering mode. Due to the presence of the dispersed phase (gas bubbles), the application of the LDA technology in multiphase flows was limited to a low-gas holdup condition. Investigations have been reported on the measurements of the liquid velocities in bubble column systems. Mudde et al.[36,37] found that both the axial and tangential liquid velocity components can be measured confidently with backscatter mode LDA in a two-phase bubble column under the condition of gas fraction ranged up to 25%.

In this work, experiments were carried out within gas holdup of 20%. The data rates from gas bubbles and other impurities varied from 15 to 30 Hz, and they were much fewer in comparison with the overall data rates (from glass tracers and gas bubbles) varied from 650 to 1,000 Hz. The overall results can be taken as those from the liquid-phase due to the order of magnitude difference between two data rates, and the similar conclusion also can be found elsewhere.[35,38]

The spherical glass particles of 10 μm in dia. with the density of 1.02×10^3 kg/m^3 were used as liquid tracers. All measurements in this study were sampled between 600 s and 900 s.

Local gas holdup measurements

Conductivity probes, employing silver-coated acupuncture needles, were used to measure local gas holdup in the bubble-column bioreactor, just as has been used by Feng et al.[35] The analog output signals of this probe were sampled by an A/D converter. Following digitization, status data were sent to the computer and stored for later analysis. A sampling time of 300 s proved satisfactory data for statistical analysis with sufficient number of samples for most conditions.

Based on the assumption that the trigger level was independent of X-directional position, a technology of self-adjusted level iterative routine and slope-phase discrimination scheme for raw signals[35, 39-40] was adopted in this work. The probe analog signal was converted into a binary signal $\delta(x,t)$, which equaled one in the gas phase and zero in the liquid phase. To digitize the signal, with total sample number N, the local time-averaged gas holdup can be expressed as

$$\varepsilon_g = \frac{1}{N} \sum_{i=1}^{N} \delta(x, t) \tag{30}$$

Phenol Biodegradation Experiments

Microorganism

The yeast *Candida tropicalis* was isolated from acclimated activated sludge, which was collected from a municipal gasworks in China. Detailed information can be found in the literature of Jiang et al..[15] The strain was identified by the Institute of Microbiology, Chinese Academy of Sciences, Beijing, China. Pure culture of yeast *Candida tropicalis* was used throughout this work.

Phenol biodegradation experiments

Batch-phenol biodegradation experiments were also carried out in the rectangle bubble-column bioreactor with *Candida tropicalis* in the liquid phase. The bubble column was sterilized with 3% hydrogen peroxide solution and washed with sterilized deionized water prior to phenol biodegradation experiments. After washing with deionized water and sterilized mineral salt medium, 24 L fermentation culture containing salt medium, the initial phenol concentration of 800–1,600 mg/L, and the initial cell concentration of 34–102 mg/L was added into the bubble column. The temperature was kept at 30°C by circulating thermostated water in the water jacket. All of the experiments were carried out at the initial pH of 6.0. The fermentation broth was sampled periodically to measure the broth concentrations of phenol and cells.

Analytical procedures

Phenol concentration was measured using high-performance liquid chromatography (HPLC, model Series III, LabAlliance, USA) equipped with a **C**18 column (250 × 4.6 mm, LabAlliance, USA). The absorbance of the effluent solution was continuously measured at 280 nm. The flow rate was 1.0 mL/min, and the mobile phase was 57.1% (V/V) of methanol. The culture broth was centrifuged at 7,500 rpm for 10 min, and the supernatant was analyzed. The retention time of phenol was 5.04 min. Cell concentration was monitored spectrophotometrically by measuring the absorbance at the wavelength of 600 nm. Cell concentration on a dry weight basis was measured by filtering the cell suspension with a filter and drying the filter article and cells to a constant weight for 24 h at 105°C. A linear relationship between dry cells weight and the optical density (OD) was obtained: cell concentration (mg/L) = $346.78 \times OD_{600} - 0.6923$. All the experiments were performed in triplicate and the average error was within ±5%.

Results and Discussion

Model validation

The proposed 3-D model can simulate the local instantaneous hydrodynamic and biodegradation behaviors of batch-phenol biodegradation processes in bubble-column bioreactor by coupling the fluid dynamic model with the kinetics of phenol biodegradation. It should be very perfect for the experimental dynamic parameters of the hydrodynamic and phenol biodegradation characteristics to be utilized for validating the developed model. However, the fermentation broth will disturb the measurement of the LDA system and conductivity probe, affecting the measurement veracity of the hydrodynamic characteristics. In order to effectively evaluate the developed model, the validation of local hydrodynamic characteristics, and the validation of phenol biodegradation behaviors were adopted, respectively. First, under the condition that no cells were added into the mineral salt medium, the developed model was simplified to the fluid dynamic model only. The measured local time-averaged and transient liquid velocities, local time-averaged gas holdups were used to validate the hydrodynamic characteristics predicted by this proposed model. Second, in the actual phenol biodegradation processes, the experimental phenol and cell concentrations were adopted to validate the dynamic behaviors of batch-phenol biodegradation processes simulated by this proposed model.

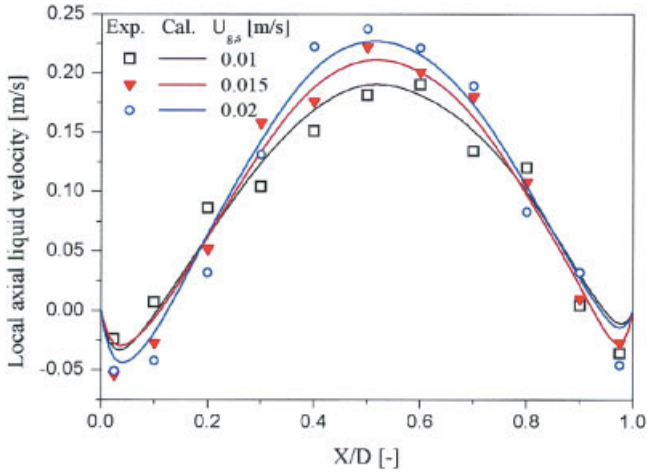

Figure 2. Simulated and experimental results of the local time-averaged axial liquid velocities with different superficial gas velocities ($u_{g,s}$), Z/D = 2.0.

[Color figure can be viewed in the online issue, which is available at www.interscience.wiley.com.]

Hydrodynamics validation

In order to validate the model simulation for the local hydrodynamic characteristics, quantitative comparisons between the measured and calculated time-averaged axial liquid velocity and gas holdup profiles of the air-mineral salts solution two-phase flow, including phenol concentration of 1,200 mg/L were performed in the bubble-column bioreactor. The effects of operating parameters, such as superficial gas velocity, axial position were also discussed. The simulated and experimental local time-averaged gas holdups were obtained from Eq. 30, and the local time-averaged axial liquid velocities were obtained directly from the LDA measurements or transient simulations by ensemble averaging as given by

$$\langle u_{l,z} \rangle = \frac{1}{N} \sum_{i=1}^{N} u_{l,z}(i) \tag{31}$$

where $u_{l,z}(i)$ represented the local axial instantaneous liquid velocity at time i, and N was the total number of samples in a sampling period.

Figures 2 and 3 showed the simulated and experimental results of the local time-averaged axial liquid velocity and gas

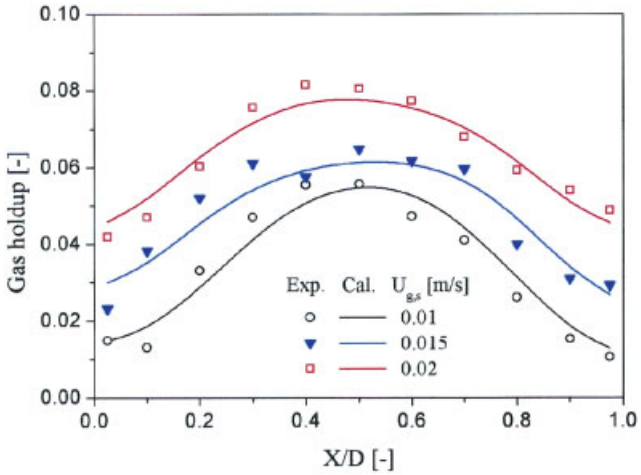

Figure 3. Simulated and experimental results of the local time-averaged gas holdups with different superficial gas velocities ($u_{g,s}$), Z/D = 2.0.

[Color figure can be viewed in the online issue, which is available at www.interscience.wiley.com.]

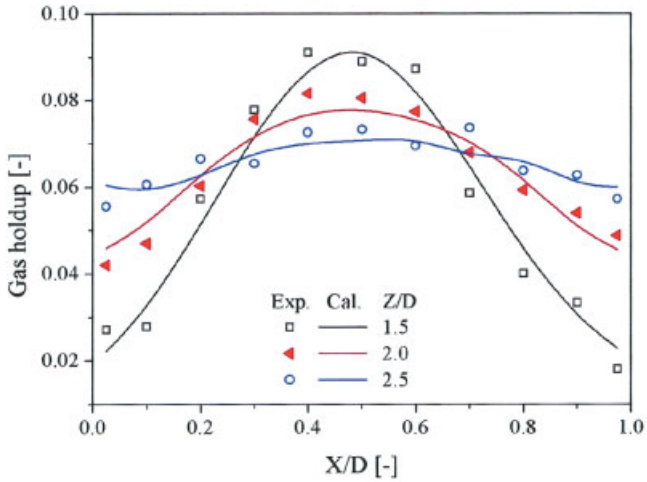

Figure 5. Comparisons of the simulated and experimental local time-averaged gas holdups at different axial positions (Z/D), $u_{g,s}$ = 0.02 m/s.

[Color figure can be viewed in the online issue, which is available at www.interscience.wiley.com.]

holdup profiles at different superficial gas velocities, respectively. It was found that the local time-averaged axial liquid velocity and gas holdup increased with increasing superficial gas velocity, and the profiles showed a manner of having a maximum in the center and a minimum near the wall. The model simulations agreed well with the experimental data.

The comparison results of the simulated and experimental local time-averaged axial liquid velocity and gas holdup profiles at different axial positions were illustrated in Figures 4 and 5. With the increase in the axial distance from the bottom, the flow became more and more uniform, and the local profiles of the time-averaged axial liquid velocity and time-averaged gas holdup became more and more flat owing to the increase of lateral mixing and momentum exchange between bubbles and the liquid phase.[41] It was clear that the simulated results were in consistent with the experimental data.

As a powerful tool, the LDA system can provide the detail transient information of the liquid velocity at a specific point in the bubble-column bioreactor. The quantitative comparison of the measured and calculated time history plot of the axial liquid velocity at one point (X = 0.02 m, Y = 0 m, Z = 0.4 m) over a time interval of 180–240 s was indicated in Figure 6. It was noted that the calculated time series of the axial liquid velocities agreed well with the measurements.

For the purpose of further quantitative comparisons, the experimental and calculated time-averaged axial liquid velocity fluctuations can be calculated as follows

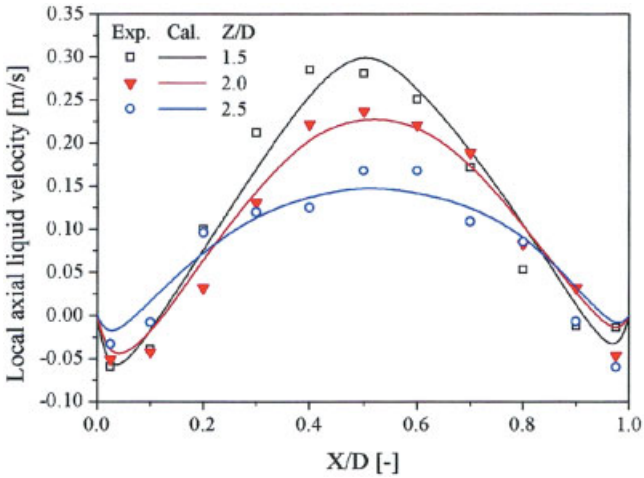

Figure 4. Comparisons of the simulated and experimental local time-averaged axial liquid velocities at different axial positions (Z/D), $u_{g,s}$ = 0.02 m/s.

[Color figure can be viewed in the online issue, which is available at www.interscience.wiley.com.]

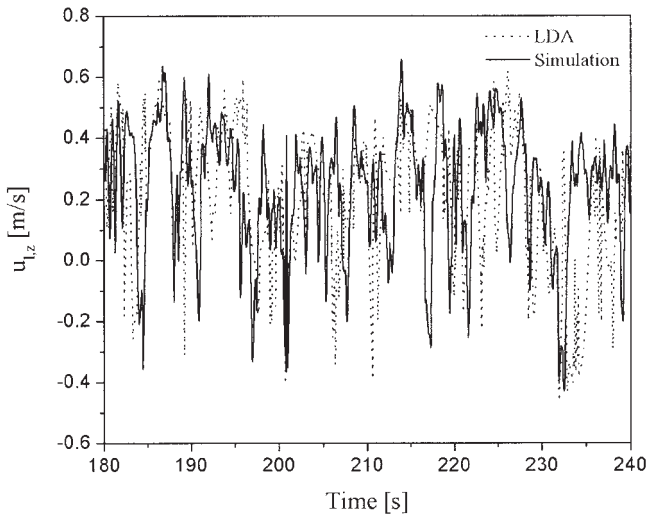

Figure 6. Time histories of modeling simulation and LDA experiment at the point of (0.02m, 0 m, 0.4m), $u_{g,s}$ = 0.02 m/s.

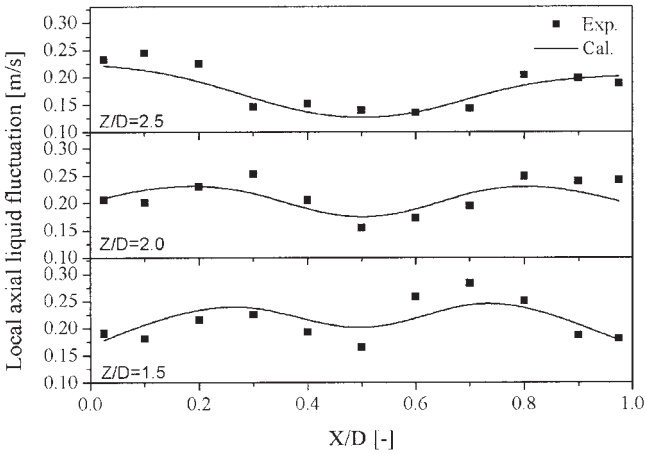

Figure 7. Comparison of simulated and experimental profiles of the time-averaged axial liquid velocity fluctuations, $u_{g,s}$ = 0.02 m/s.

$$\langle u'_{l,z}\rangle = \left(\frac{1}{N}\sum_{i=1}^{N}\left(u_{l,z}(i) - \langle u_{l,z}\rangle\right)^2\right)^{0.5} \tag{32}$$

Comparison results were demonstrated in Figure 7. It was observed that the minimum axial liquid fluctuations occurred in the center area, which is in correspondence with the LDA experimental results of Deen.[23] In addition, Figure 7 also showed that the maximum axial liquid fluctuations moved toward the walls along the axial direction, which was also validated nicely by the experimental data.

From Figures 2–7, it can be observed that the simulated local hydrodynamic characteristics agreed well with the experimental data, indicating that the proposed model could be convincingly used to predict the hydrodynamic behaviors of the bubble-column reactor in the absence of bioreaction.

Validation of phenol biodegradation behavior. To investigate the dynamic behaviors of phenol biodegradation by yeast *Candida tropicalis,* and to validate the proposed model, the simulated results and experimental data of phenol biodegradation in the 40 L bubble-column bioreactor were obtained and compared. Effects of different superficial gas phase velocities, initial phenol concentrations and initial cell concentrations on the degree of phenol biodegradation were investigated at the centerline of the column, at a height of $Z/D = 2.0$.

Figure 8 showed the influences of the superficial gas velocities on the distributions of the cell and phenol concentrations with time under the conditions, such as the initial phenol concentration of 1,200 mg/L and initial cell concentration of 68 mg/L. It was evident that the presence of superficial gas phase velocities resulted in the increase of cell concentration, and the decrease of phenol concentration comparing with the intrinsic ones due to the effect of the hydrodynamic characteristics. The cell concentration slightly increased and phenol concentration slightly decreased with increasing in the superficial gas velocities. It was also observed that the simulated results were in good correspondence with the experimental data.

Figure 9 was the effects of different initial phenol concentrations on the simulated and experimental profiles of cell and phenol concentrations at the fixed initial cell concentration of

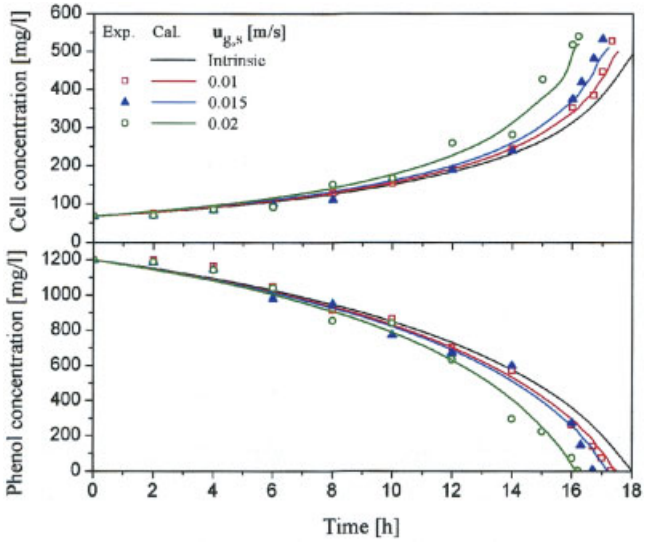

Figure 8. Simulated and experimental profiles of the cell and phenol concentrations at different superficial gas phase velocities ($u_{g,s}$), $C_{S,0}$ = 1,200 mg/L, $C_{X,0}$ = 68 mg/L.

[Color figure can be viewed in the online issue, which is available at www.interscience.wiley.com.]

68 mg/L. It can be seen that the initial phenol concentration of 800, 1,200 and 1,600 mg/L could be completely degraded by yeast *Candida tropicalis* within 11.5, 16.5 and 21.8 h, respectively. It was attributed to the fact that, with the increase of initial phenol concentration, the effect of the substrate inhibition increased remarkably, especially at the high phenol concentration.[42] It also revealed that the experimental data agreed well with the simulated results.

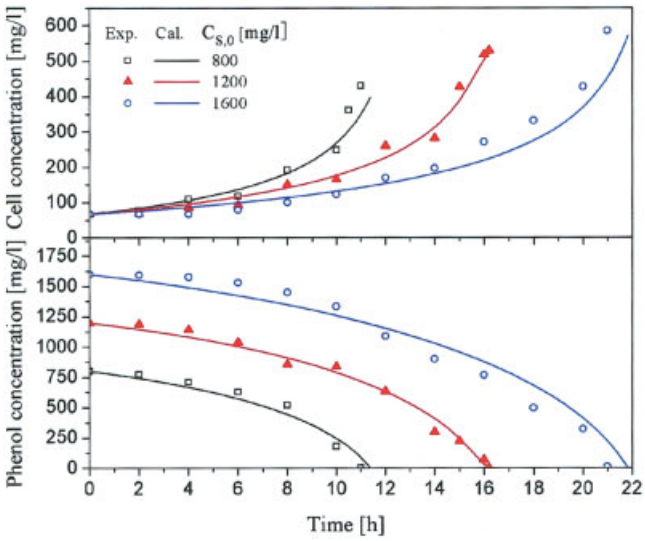

Figure 9. Effects of different initial phenol concentrations ($C_{S,0}$) on the simulated and experimental profiles of cell and phenol concentrations, $C_{X,0}$ = 68 mg/L, $u_{g,s}$ = 0.02 m/s.

[Color figure can be viewed in the online issue, which is available at www.interscience.wiley.com.]

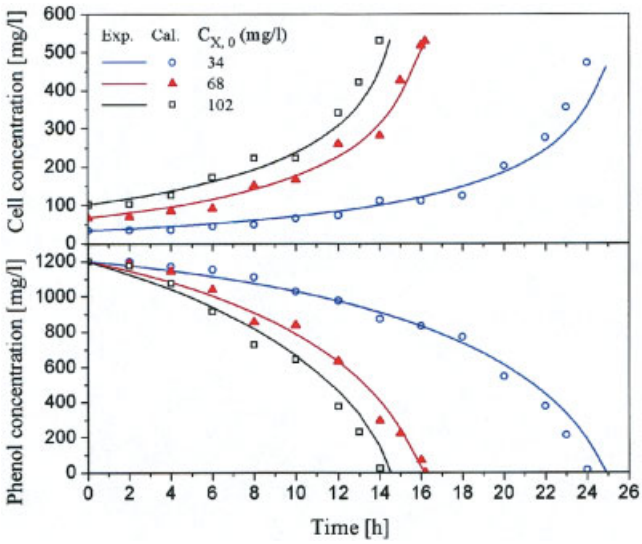

Figure 10. Simulated and experimental profiles of cell and phenol concentrations as a function of the initial cell concentrations ($C_{X,0}$), $C_{S,0}$ = 1,200 mg/L, ug,s = 0.02 m/s.

[Color figure can be viewed in the online issue, which is available at www.interscience.wiley.com.]

The typical results of cell and phenol concentrations as functions of the initial cell concentrations at the same initial phenol concentration of 1,200 mg/L were given in Figure 10, respectively. With the increase in initial cell concentration, the capability of cells to overcome the substrate inhibition increased, and manifested higher phenol-degrading velocity. Phenol was entirely degraded within 25 h at the initial cell concentration of 34 mg/L, which was 8.8 h and 10.4 h longer than that at the initial cell concentrations of 68 and 102 mg/L, respectively. The reason may be the result from the fact that more cells would consume more phenol and then more nutrients (including phenol) in broth is utilized to synthesize new cells.[15] It can be observed that the calculated results of cell and phenol concentrations were in reasonable agreement with experimental data.

From Figures 8–10, it was clear that the agreements between the simulated results and corresponding experimental data of phenol and cell concentration profiles in the bubble column bioreactor were very good. It is indicated that this proposed model can be adopted for simulating the dynamic behaviors of batch phenol biodegradation processes using free cells of the yeast *Candida tropicalis* in the bubble-column bioreactor effectively.

Model Prediction

Lab-scale model prediction

It was very necessary and important that the developed model was used to predict the local instantaneous flow and phenol biodegradation features in the bubble-column bioreactor. Snapshots of the local instantaneous gas holdup, gas velocity, liquid velocity, phenol concentration and cell concentration under the condition of superficial gas phase velocity of 0.02 m/s, initial phenol concentration of 1,600 mg/L, and initial cell concentration of 68 mg/L in a lab-scale bubble-column bioreactor were shown in Figure 11.

It can be observed that the flow is driven by a bubble plume moving through the column in an oscillatory manner. Large vortices alongside the bubble plume are engendered not only in the liquid velocity fields, but also in the gas velocity fields, and the bubbles were carried downward by the liquid circumfluence. Such unsteady flow behaviors have been experimentally observed by Becker et al.[43] and Chen et al..[44]

Phenol concentrations in the bubble-column bioreactor were almost uniform because of high-efficient interphase mixing. However, for each snapshot of the phenol concentration field, there still was a very little difference in the values of the phenol concentrations which should be caused by the transient flow behaviors. Furthermore, it was also seen that the transient distributions of the phenol concentration field were in relation to the corresponding transient flow fields. Same phenomenon also can be found in the cell fields due to the full coupling of flow and bioreaction.

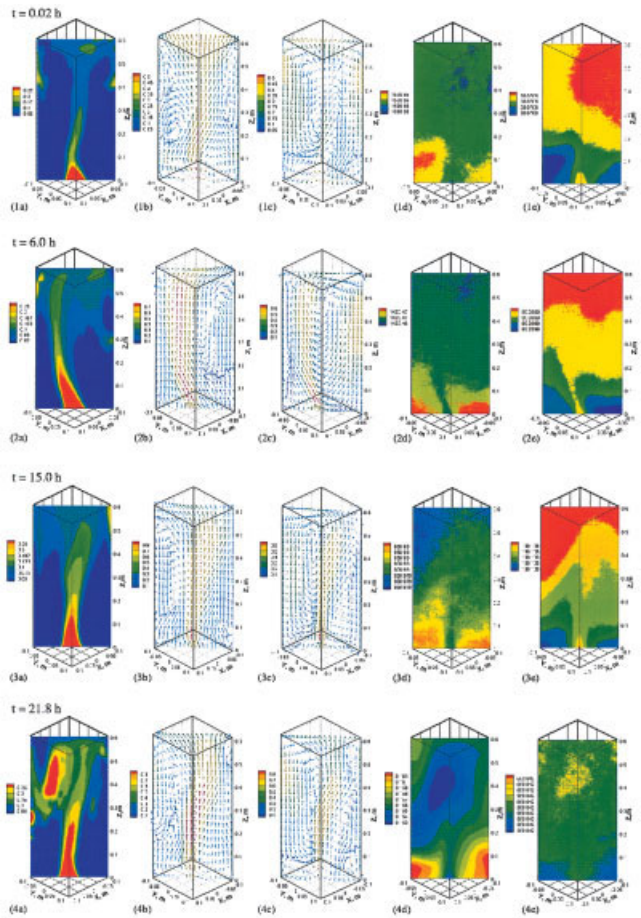

Figure 11. Transient model predictions of lab-scale bubble column (a) gas holdup, (b) gas velocity, (c) liquid velocity, (d) phenol concentration, and (e) cell concentration at the time of (1) 0.02 h, (2) 6.0 h, (3) 15.0 h, (4) 21.8 h, $u_{g,s}$ = 0.02 m/s, $C_{S,0}$ = 1600 mg/L,. $C_{X,0}$ = 68 mg/L.

[Color figure can be viewed in the online issue, which is available at www.interscience.wiley.com.]

With the proceeding of phenol biodegradation by yeast *Candida tropicalis*, the concentration of phenol decreased, and the cell concentration increased, leading to the fact that liquid density decreased and the surface tension of the liquid phase increased gradually according to Eq. 23 and Eq. 25. Thus, the coalescence efficiency of small bubbles in the bioreactor enhanced with the proceeding of phenol biodegradation, which resulted in a slight increase of the local transient gas velocity and a slight decrease of the local instantaneous gas holdup as shown in Figure 11.

Large-scale model prediction

Because of their complex hydrodynamics, large-scale bubble columns have gained considerable attentions in recent years. The traditional scale-up methods usually depended on empirical guidelines, scale-up rules and dimensional analysis.[45] With the development of CFD technology, the dynamic simulation and model prediction will play an important role in the design and scale-up of bubble-column reactors.

Instantaneous predictions of the hydrodynamic characteristics and phenol biodegradation behaviors were also carried out in a virtual square large-scale bubble-column bioreactor, with the size of $2 \times 2 \times 6$ m, where a square gas distributor plate, centrally located at the bottom of the column, was 0.5 m in width and contained 16,900 holes with the diameter of 1.0 mm. The predictions of the earlier large-scale bubble column were under the same operation conditions as the lab-scale one, namely, superficial gas velocity of 0.02 m/s, initial phenol concentration of 1,600 mg/L and initial cell concentration of 68 mg/L. The snapshots were shown in Figure 12.

From the hydrodynamics predictions in Figure 12, it was found that the flow structures in the large-scale bubble column were more regular than those of the lab-scale one, and there were three main regions in the large-scale bubble-column reactor, the up-flowing region in the center area (Region I), the descending flow region near the wall (Region II), and the transition region (Region III) between above two regions. In Region I, the gas and liquid velocities were much higher than those of the lab-scale bubble-column bioreactor, which may be attributed to the fact that more large bubbles occurred in the bubble up-flowing region.[46,47] In Region II, bubbles were dragged and carried downward by the liquid phase, the liquid and gas phases flowed downward, showing that the liquid and gas velocities are negative. In Region III, some gas vortices in the air velocity fields, and the liquid circumfluence in the liquid velocity fields were seen.

From the predictions of the phenol biodegradation in Figure 12, more obvious nonuniform concentration profiles of phenol and cell were observed in the large-scale bubble column, than those in lab-scale bubble column. However, the differences in phenol and cell concentration distributions were still very small, and it may be due to the fact that the bioreaction was the controlling step compared to the fluid flow in the proceeding of phenol biodegradation.

Conclusion

In this work, a coupled 3D model, combining hydrodynamics with biochemical reaction, was developed for the predictions of the flow patterns and phenol biodegradation behaviors

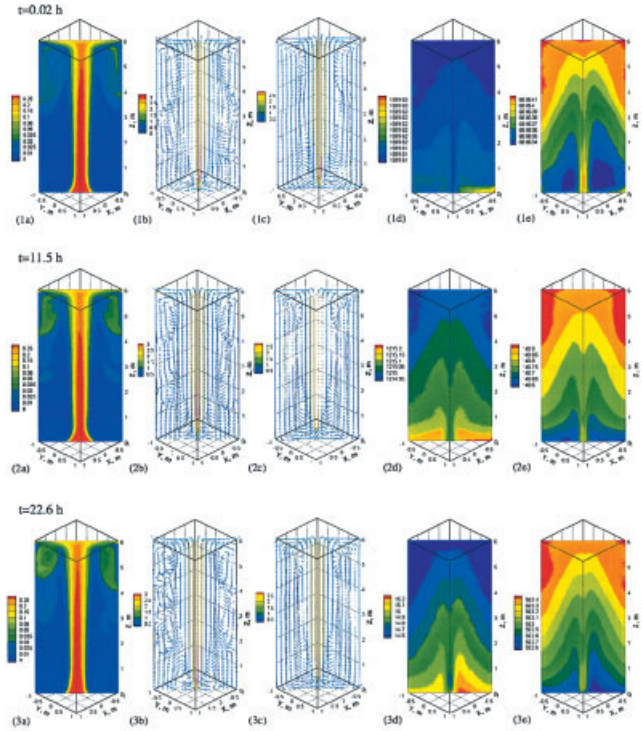

Figure 12. Transient model predictions of large-scale bubble column: (a) gas holdup, (b) gas velocity, (c) liquid velocity, (d) phenol concentration, and (e) cell concentration at the time of (1) 0.01 h, (2) 11.5 h, (3) 22.6 h, $u_{g,s}$ = 0.02 m/s, $C_{S,o}$ = 1,600 mg/L,. $C_{X,o}$ = 68 mg/L.

[Color figure can be viewed in the online issue, which is available at www.interscience.wiley.com.]

by yeast *Candida tropicalis* in the bubble-column bioreactor. In order to validate the proposed model more effectively, the validation of hydrodynamic characteristics and the validation of dynamic phenol biodegradation behaviors were adopted, respectively.

The hydrodynamic validation of the air-mineral salts solution two-phase flow including phenol concentration of 1,200 mg/L was performed in a square-sectioned bubble-column bioreactor using LDA and conductivity probe. It was found that the simulated and experimental local time-averaged axial liquid velocity, and local time-averaged gas holdup increased with increasing superficial gas velocity, and decreased with increasing axial distance from the bottom of the bubble column, which were in correspondence with the tendencies of traditional gas-liquid two-phase fluidization. The model simulation results were in good agreement with the experimental data.

The validation of phenol biodegradation behaviors by yeast *Candida tropicalis* under different initial concentrations of phenol and cell was carried out in the same bubble-column bioreactor. With the increase of initial cell concentration and the decrease of initial phenol concentration, the simulated and experimental cell concentration increased and phenol concentration decreased. In addition, the effects of superficial gas velocities on the profiles of cell and phenol concentrations with time were also investigated. The presence of superficial gas velocity enhanced the cell growth and phenol biodegradation

comparing with the intrinsic ones. The model simulations of cell and phenol concentration profiles were in reasonable consistency with the experimental data.

Finally, the lab-scale and large-scale of modeling predictions of the local instantaneous flow structures including phenol biodegradation behaviors such as gas holdup, gas velocity, liquid velocity, phenol concentration and cell concentration at different time in the process of phenol biodegradation by yeast *Candida tropicalis* were successfully predicted by this proposed model, which will provide the strategies for the optimum design and scale-up of the bubble-column bioreactors.

Acknowledgments

The authors wish to acknowledge the financial support provided by the Key National Natural Science Foundation of China (No. 20336030), Key Natural Science Foundation of Tianjin (No. 05YFJZJC 00500), Program for science and technology development of Tianjin (No. 043185111-20), Program for New Century Excellent Talents in University and Program for Changjiang Scholars and Innovative Research Team in University.

Notation

C_D = drag coefficient, dimensionless
C_L = lift coefficient, constant, 0.76
C_{VM} = virtual mass coefficient, constant, 0.5
C_μ = constant, 0.09
$C_{\mu,BIT}$ = constant, 0.6
C_{TD} = turbulent dispersion coefficient, constant, 0.3
d_B = Sauter mean bubble diameter, mm
D = the side length of the square cross-sectioned bubble-column reactor, 0.2 m
$Eö$ = Eötvös number ($= g\Delta\rho d_B^2/\sigma$), dimensionless
f_k = mass fraction of ***kth*** species in the liquid phase, dimensionless
F_1 = blending function
F_2 = second blending function
$\mathbf{g}$ = gravitational acceleration, = 9.81 m/s^2
H = height in axial direction (Z-direction)
H/D = dimensionless axial position
$\mathbf{M}_D$ = drag force per unit volume, N/m^3
$\mathbf{M}_I$ = interface force between the gas phase and suspension phase, N/m^3
$\mathbf{M}_L$ = lift force per unit volume, N/m^3
$\mathbf{M}_{MV}$ = virtual mass force per unit volume, N/m^3
$\mathbf{M}_{TD}$ = turbulent dispersion force per unit volume, N/m^3
P = pressure, Pa
Re_B = bubble Reynolds number, dimensionless
S = phenol concentration, mg/L
$[S]$ = unit concentration of phenol, mg/L
S_{inlet} = area of gas inlet, m^2
Sc = Schmidt number ($= \mu_{L,l}/(\rho_l D)$), dimensionless
T = temperature, K
t = time, s
$\mathbf{u}_g$ = gas velocity, m/s
$u_{g,s}$ = superficial gas velocity, m/s
$\mathbf{u}_i$ = velocity of ***i*th** phase, m/s
$\mathbf{u}_l$ = liquid velocity, m/s
$u_{l,z}$ = local axial liquid velocity; liquid velocity component of Z-direction, m/s
$\langle u_{l,z}\rangle$ = time-averaged axial liquid velocity, m/s
$\langle u'_{l,z}\rangle$ = time-averaged axial liquid velocity fluctuation, m/s
u_{slip} = slip velocity, m/s
X = X-direction position, m; cell concentration, mg/L
$[X]$ = unit concentration of cell, mg/L
X/D = dimensionless transversal position, m
Y = Y-direction position, m
Z = Z-direction (axial) position, m

Greek letters

α_1 = constant, 5/9
α_2 = constant, 0.44
β_1 = constant, 3/40
β_2 = constant, 0.0828
β' = constant, 0.09
ε = volume fraction, dimensionless
ε_i = volume fraction for ***i*th** phase, dimensionless
μ = viscosity, kg/m · s
$\mu_{l,0}$ = viscosity of the mineral salt medium without phenol and cells, kg/m · s
ρ = density, kg/m^3
$\rho_{l,0}$ = liquid density of the mineral salt medium without phenol and cells, kg/m^3
σ = surface tension, N/m
$\sigma_{l,0}$ = surface tension of the mineral salt medium without phenol and cells, N/m
σ_{k1} = constant, 0.85
σ_{k2} = constant, 1
$\sigma_{\omega 1}$ = constant, 2
$\sigma_{\omega 2}$ = constant, 1/0.856.
δ = binary signal converted from the conductivity probe signal, dimensionless
Υ = the source term accounting for the production rate or biodegradation rate

Subscripts and superscripts

B = bubble
cell = cells
D = drag
eff = effective
g = gas phase
i = ***i*th** phase
inlet = gas inlet
l = liquid phase
L = lift; laminar
phenol = phenol
s = superficial
S = phenol
VM = virtual mass
TD = turbulent dispersion
X = cell

Literature Cited

1. Hannaford AM, Kuek C. Aerobic batch degradation of phenol using immobilized Pseudomonas putida. *J Ind Microbiol Biot*. 1999;22:121-126.
2. Nuhoglu A, Yalcin B. Modelling of phenol removal in a batch reactor. *Process Biochem*. 2005;40:1233-1239.
3. Yang RD, Humphrey AE. Dynamic and steady state studies of phenol biodegradation in pure and mixed cultures. *Biotechnol Bioeng*. 1975; 17:1211-1235.
4. Caldeira M, Heald SC, Carvalho MF, Vasconcelos I, Bull AT, Castro PML. 4-Chlorophenol degradation by a bacterial consortium: Development of a granular activated carbon biofilm reactor. *Appl Microbiol Biot.* 1999;52:722-729.
5. Fang HHP, Zhou GM. Denitrification of phenolic wastewater by immobilized sludge. *Environ Technol*. 1997;18:827-834.
6. Holub W, Przytocka-Jusiak M, Blaszczyk M, Mycielski R. Nitrite as agent selecting anaerobic phenol-degrading microflora in petroleum refining sediments. *Water Res*. 2000;34:1354-1358.
7. Sarfaraz S, Thomas S, Tewari UK, Iyengar L. Anoxic treatment of phenolic wastewater in sequencing batch reactor. *Water Res*. 2004;38: 965-971.
8. Sutton PW, Mishra PN. Activated carbon based biological fluidized beds for contaminated water and wastewater treatment: A state-of-the-art review. *Water Sci Technol*. 1994;29:309-317.
9. Jiang HL, Tay JH, Maszenan AM, Tay STL. Bacterial diversity and function of aerobic granules engineered in a sequencing batch reactor for phenol degradation. *Appl Environ Microb*. 2004;70:6767-6775.
10. Watanabe K, Teramoto M, Harayama S. An outbreak of nonflocculation catabolic populations caused the breakdown of a phenol-digesting activated sludge process. *Appl Environ Microb*. 1999;65:2813-2819.
11. Ha SR, Vinitnantharat S. Competitive removal of phenol and 2,4-

dichlorophenol in biological activated carbon system. *Environ Technol*. 2000;21:387-396.
12. Li, PHY, Roddick FA, Hobday MD. Bioregeneration involving a coal-based adsorbent used for removing nitrophenol from water. *J Chem Technol Biot*. 1998;73:405-413.
13. Santos VL, Linardi VR. Biodegradation of phenol by a filamentous fungi isolated from industrial effluents-identification and degradation potential. *Process Biochem*. 2004;39:1001-1006.
14. Vinitnantharat S, Baral A, Ishibashi Y, Ha SR. Quantitative bioregeneration of granular activated carbon loaded with phenol and 2,4-dichlorophenol. *Environ Technol*. 2001;22:339-344.
15. Jiang Y, Wen JP, Li HM, Yang SL, Hu ZD. The biodegradation of phenol at high initial concentration by the yeast *Candida tropicalis*. *Biochem Eng J*. 2005;24:185-277
16. Gonzalez G, Herrera MG, Garcia MT, Pena MM. Biodegradation of phenol in a continuous process: comparative study of stirred tank and fluidized-bed bioreactors. *Bioresource Technol*. 2001;76:245-251.
17. Raja Rao TBML, Sonolikar RL, Pentu Saheb S. Influence of magnetic field on the performance of bubble columns and airlift bioreactor with submersed microorganisms. *Chem Eng Sci*. 1997;52:4155-4160.
18. Ruiz-Ordaz N, Ruiz-Lagunez JC, Castañón-Gonzaález JH, Hernández-Manzano E, Cristiani-Urbina E, Galíndez-Mayer J. Phenol Biodegradation Using a Repeated Batch Culture of *Candida tropicalis* in a Multistage Bubble Column. *Revista Latinoamericana de Microbiologia*. 2001;43:19-25.
19. Tay J-H, Jiang H-L, Tay ST-L. High-rate biodegradation of phenol by aerobically grown microbial granules. *J Environ Eng*. 2004;130:1415-1423.
20. Monteiro AMG, Boaventura AR, Rodrigues AE. Phenol biodegradation by Pseudomonas putida DSM 548 in a batch reactor. *Biochem Eng J*. 2000.6, 45-49.
21. Livingston AG, Chase HA. Modeling phenol degradation in a fluidized-bed bioreactor. *AIChE J*. 1989;35:1980-1992.
22. Darmana D, Deen NG, Kuipers JAM. Detail modeling of hydrodynamics, mass transfer and chemical reactions in a bubble column using a discrete bubble model. *Chem Eng Sci*. 2005;60:3383-3404.
23. Deen NG. *An experimental and computational study of fluid dynamics in gas-liquid chemical reactors*. Aalborg University, Esbjerg; 2001. PhD Thesis.
24. Delnoij E., Kuipers J.A.M., van Swaaij W.P.M.. A three-dimensional CFD model for gas-liquid bubble columns. *Chem Eng Sci*. 1999;54: 2217-2226;
25. Jakobsen HA, Sannaes BH, Gervskott S, Svendsen HF. Modeling of vertical bubble-driven flows. *Ind Eng Chem Res*. 1997;36:4052-4074.
26. Machon V, Pacek AW, Nienow AW. Bubble sizes in electrolyte and alcohol solutions in a turbulent stirred vessel. *Chem Eng Res Des*. 1997;75:339-348.
27. Calderbank PH. Physical Rate Processes in Industrial Fermentation. Part I: The interfacial area in gas-liquid contacting with mechanical agitation. *Trans Inst Chem Eng*. 1958;36:443-463.
28. Tsuchiya K, Furumoto A, Fang L-S, Zhang J. Suspension viscosity and bubble rise velocity in liquid-solid fluidized beds. *Chem Eng Sci*. 1997;52:3053-3066.
29. Lopez de Bertodano MA. Two-fluid model for two-phase turbulent jet. *Nucl Eng Des*. 1998;179:65-74.
30. Menter FR, Kuntz M, Langtry R. Ten years of industrial experience with the SST turbulence model. In: Hanjalic K, Nagano Y, Tummers MJ. *Turbulence, Heat and Mass Transfer 4*. Begell House, Inc.; 2003:625-632.
31. Sato Y, Sekoguchi K. Liquid velocity distribution in two-phase bubble flow. *Int J Multiphase Flow*. 1975;2:79-95.
32. Cao JY, Wen JP. Fluid hydrodanymics and physical properties of phenol biodegradation in bioreactors.. Tianjin University, 2005.
33. *CFX Flow Solver User Guide*. Computational Fluid Dynamics Services, ANSYS Canada, Ltd.; 2003. Bachelor Dissertation.
34. Krishna R, van Baten JM, Urseanu MI, Ellenberger J. Design and scale up of a bubble column slurry reactor for Fisch-Tropsch synthesis. *Chem Eng Sci*. 2001;56:537-545.
35. Feng W, Wen JP, Fan JH, Yuan Q, Jia XQ, Sun Y. Local hydrodynamics of gas-liquid-nanoparticles three-phase fluidization. *Chem Eng Sci*. 2005;60:6887-6898.
36. Mudde RF, Groen JS, Van Den Akker HEA. Liquid velocity field in a bubble column: LDA experiments. *Chem Eng Sci*. 1997;52:4217-4224.
37. Mudde RF, Groen JS, Van Den Akker HEA. Application of LDA to bubbly flows. *Nucl Eng Des*. 1998;184:329-338.
38. Cui Z, Fan L-S. Turbulence energy distributions in bubbling gas-liquid and gas-liquid-solid flow systems. *Chem Eng Sci*. 2004;59:1755-1766.
39. Liu T J, Bankoff SG. Structure of air water bubbly flow in a vertical pipe - II. Void fraction, bubble velocity and bubble size distribution. *Int J Heat Mass Tran*. 1993;36:1061-1072.
40. Wen JP. *Local study on flow, mass transfer and franctals in the self-aspirated reversed flow jet loop reactor*. Tianjin University Tianjin, P. R. China; 1995. PhD. Thesis.
41. Wen JP, Xu ShL. Local hydrodynamics in a gas-liquid-solid three-phase bubble column reactor. *Chem Eng J*. 1998;70:81-84.
42. Claußen M, Schmidt S. Biodegradation of phenol and P-cresol by the hyphomycete Scedosporium apiospermum. *Res Microbiol*. 1998;149: 399-406.
43. Becker S, Sokolichin A, Eigenberger G. Gas-liquid flow in bubble columns and loop reactors: part II. Comparison of detailed experiments and flow simulations. *Chem Eng Sci*. 1994;49:5747-5762.
44. Chen RC, Reese J, Fan L-S. Flow structure in a three-dimensional bubble column and three-phase fluidized bed. *AIChE J*. 1994;40:1093-1104.
45. Kantarci, N, Borak, F, Ulgen, KO. Bubble column reactors. *Process Biochem*. 2005; 40:2263-2283
46. Li H, Prakash A. Influence of slurry concentrations on bubble population and their rise velocities in three-phase slurry bubble column. *Powder Technol*. 2000;113:158-67.
47. Koide K, Morooka S, Ueyama K, Matsuura A. Behavior of bubbles in large scale bubble column. *J Chem Eng Jpn*. 1979;12:98-104.

Manuscript received Nov. 8, 2005, and revision received Mar. 31, 2006.